Nanoscale

Accepted Manuscript

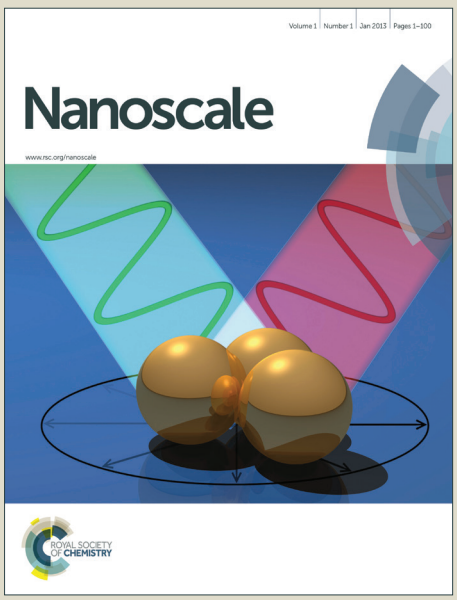

ROYAL SOCIETY OF CHEMISTRY

www.rsc.org/nanoscale

Nanoscale

RSCPublishing

PAPER

Highly reproducible planar Sb_2S_3-sensitized solar cells based on atomic layer deposition

Cite this: DOI: 10.1039/x0xx00000x

§Dae-Hwan Kim[a], §Sang-Ju Lee[a], Mi Sun Park[a], Jin-Kyu Kang[a], Jin-Hyuk Heo[b], Sang Hyuk Im[b]*, Shi-Joon Sung[a]*

Received 00th January 2013,
Accepted 00th January 2013

DOI: 10.1039/x0xx00000x

www.rsc.org/

A high-quality Sb_2S_3 thin-absorber with controllable thickness was reproducibly formed by atomic layer deposition (ALD) technique. Compared with conventional chemical bath deposition (CBD), the Sb_2S_3 absorber deposited by ALD did not contain oxide or oxygen impurities and showed very uniform thickness of Sb_2S_3 absorbers formed on rough surface of dense blocking TiO_2/F-doped SnO_2 (bl-TiO_2/FTO) substrate. The planar ALD-Sb_2S_3 solar cells comprised to Au/Poly-3-hexylthiophene/ALD-Sb_2S_3/bl-TiO_2/FTO showed greatly improved power conversion efficiency of 5.77 % at 1 sun condition and narrow efficiency's deviation whereas the planar CBD-Sb_2S_3 solar cells exhibited 2.17 % of power conversion efficiency. The high efficiency and good reproducibility of ALD-Sb_2S_3 solar cell devices is attributed to the reduced backward recombination due to the inhibition of oxide defects within ALD-Sb_2S_3 absorber and the conformal deposition of very uniform Sb_2S_3 absorbers on blocking TiO_2 surface by ALD process.

Introduction

The second generation solar cells such as organic, thin-film, and dye-sensitized solar cells (D-SSCs) have been intensively studied to satisfy the criteria of high efficiency and low cost. Among them, the D-SSCs have been considered as promising candidate of replacing conventional silicon solar cells owing to their unique device architecture comprised to electron conductor, sensitizer, and hole conductor because the generated electrons (holes) in sensitizer by light illumination are immediately transported into electron (hole) conductor and consequently less recombination will be expected. Therefore the sensitized solar cells (SSCs) have attracted great attention since Grätzel *et al.*[1] reported the liquid type D-SSCs and the power conversion efficiency of D-SSCs reaches to ~13% at 100 mW/cm^2 AM1.5G.[2]

Recently inorganic semiconductors and quantum dots (QDs) have been of great interest because they can replace the conventional Ru/organic dyes owing to their unique properties such as strong absorptivity, large dielectric constant, multiple exciton generation, and good stability.[3,4] Hence many metal chalcogenides including CdS(e),[5-8] PbS(e),[9-11] and $Sb_2S(e)_3$[12-18] have been used as new sensitizer and their device efficiencies have been stiffly increased up to over 7% at 1 sun condition.[19] Among them, the Sb_2S_3 exhibited peculiar characteristics of which it forms amorphous phase on the TiO_2 electrode at initial processing stage and it is then converted to crystalline stibnite by subsequent heat treatment. This may lead the formation of intimate junction at TiO_2-Sb_2S_3 interface and thus enables the Sb_2S_3-SSCs to hold high device efficiencies.

So far, the Sb_2S_3 has been synthesized by aqueous based chemical bath deposition (CBD) method[20] to form conformal thin-film on the TiO_2 electrode. Therefore the formation of antimony oxides cannot be avoided through the conventional aqueous phase CBD technique and the further improvement of device performance seem to be retarded because the antimony oxides make deep traps in the gap state and consequently causes the backward recombination of generated charge carriers[21]. Recently, Maiti *et al.*[22] reported the non-aqueous phase CBD technique for the formation of Sb_2S_3 by using single source precursor and proved the significant depression of the formation of antimony oxides. Very recently, Choi *et al.*[19] demonstrated that the antimony oxides formed by conventional CBD method can be recovered into Sb_2S_3 by post organic sulfur treatment. Hence it is prerequisite to the formation of pure Sb_2S_3 through certain deposition process in order to develop efficient Sb_2S_3-SSCs.

It is also equally important to develop highly reproducible Sb_2S_3-SSCs with narrow deviation of device efficiency. To make very reproducible Sb_2S_3-SSCs, the uniform thickness control of Sb_2S_3 light absorber is crucial. From this aspect, the conventional CBD method has intrinsic disadvantage because the thickness of Sb_2S_3 is greatly depended on the heterogeneous nucleation and growth process by chemical reaction and consequently its thickness is not linearly dependent on the reaction time. Meanwhile, the atomic layer deposition (ALD) is very powerful technique to linearly control the thickness of thin films and recently Wedemeyer *et al.*[23] demonstrated the possibility of ALD technique to form uniform Sb_2S_3 layer. Therefore, here we adapted ALD technique to precisely control the thickness of Sb_2S_3 layer and to form the pure Sb_2S_3 phase. Through the systematic thickness control of Sb_2S_3 layer, we could

demonstrate the highly reproducible planar Sb_2S_3-SSCs with 5.77 % of power conversion efficiency at 1 sun illumination.

Experimental

The amorphous Sb_2S_3 was initially obtained by the ALD of tris-dimethylamino antimony ($Sb(N(CH_3)_2)_3$; UP Chemical Co., Ltd.) and H_2S (99.5%, Matheson) gas onto a FTO/bl-TiO_2 substrate (15 Ω/cm, Pilkington) in a showerhead type ALD system (CN1 Co., Ltd, ATOMIC PREMIUM) at 130 °C. The bl-TiO_2 layer of ~70 nm thickness was deposited by spray pyrolysis and annealed at 450 °C. Pulse, exposure, and purge times of $(Sb(N(CH_3)_2)_3$ are 0.5s, 10s, and 10s; Pulse and purge times of H_2S are 3s and 10s.

To convert the amorphous phase to crystalline one, the atomic layer deposited yellowish films of amorphous Sb_2S_3/bl-TiO_2/FTO were annealed at 330 ℃ for 30 min under H_2S gas. After annealing, dark-brown crystalline stibnite Sb_2S_3/bl-TiO_2/FTO was removed from the heater immediately and cool down under N_2. As an organic hole transporting material (HTM), poly-3-hexylthiophene (P3HT; Rieke metals, Inc) was used. The solution of the HTM (15 mg/mL in 1,2-dichlorobenzene) was spin-coated onto the dense TiO_2/Sb_2S_3 layer with 2500 rpm for 60 s. Then, in order to improve the contact between P3HT and Au, a poly(3-4-ethylenedioxythiophene) doped with poly(4-styrenesulfonate) (PEDOT:PSS; Baytron AI4083) diluted with six volumes of 2-propanol was spin-coated onto the P3HT/Sb_2S_3/bl-TiO_2 at 2000 rpm for 30 s. In order to form a hybrid heterojunction, the dense TiO_2/Sb_2S_3/P3HT/PEDOT:PSS layer was annealed at 90 °C for 30 min in vacuum oven. Finally the counter electrode was deposited by thermal evaporation of gold under a pressure of 5×10^{-6} Torr giving an active area of 0.16 cm^2 for each device.

J-V data were measured using a solar simulator (Newport, 94022A) at 1 sun (AM 1.5G, 100 mW cm^{-2}) and under varied intensity of illumination by a source meter (Keithley 2400) equipped with a calibrated Si-reference cell (certified by NREL). The external quantum efficiencies (EQE) of solar cells were analyzed using an Incident Photon-to-Current Efficiency (IPCE) measurement system (McScience co., LTD, K3100) consisting of a 300-W xenon lamp, a monochromator (Spectral Products, CM110), and a multimeter (Keithley 2400). In order to eliminate experimental errors, four different cells with the same structure were fabricated using the same procedure, and all measurements were carried out five times and averaged. Photovoltaic performance was measured by using a metal mask with an aperture area of 0.096 cm^2.

Ellipso Technology Elli-SE-aM8 variable angle spectroscopic ellipsometer was used to obtain the thickness of the Sb_2S_3 thin film and confirmed by FE-SEM (Hitachi SU8020). The UV-visible diffuse absorbance spectra of the Sb_2S_3 films were obtained using a Perkin Elmer Lambda 750 UV/VIS spectrometer with an integrating sphere. XPS spectra were acquired with an ESCALAB 250Xi (Thermo Scientific, UK) system by using a microfocused (500 ㎛, 157 W) Al Kα X-ray beam with a photoelectron takeoff angle of 90º. A dual-beam charge neutralizer (1 eV Ar^+ and 1 eV electron beams) was used to compensate for the charge-up effect. Ar^+ ion source was operated at 3 μA and 2 kV, with rastering on an area of 4 mm × 2 mm. XPS spectra of the CBD-Sb_2S_3 and ALD-Sb_2S_3 were obtained after Ar sputtering for 60s. The cross-sectional morphology of the device was measured by FE-TEM (Hitachi, HF3300) with FIB systems (NB5000).

Results and discussion

Figure 1 shows a schematic illustration of the formation of Sb_2S_3 layer on the blocking TiO_2 (bl-TiO_2)/FTO (F doped SnO_2) substrate by conventional CBD and ALD process. In CBD process as illustrated in Figure 1a, the thickness of Sb_2S_3 layer is determined by the rate of chemical reaction and thus the precise temperature control of the reaction bath is very important. In addition, it is very difficult to reproducibly make uniform thickness of Sb_2S_3 layer even in the same reaction process because the heterogeneous nucleation condition of Sb_2S_3 on bl-TiO_2/FTO substrate will depend on the surface state of bl-TiO_2/FTO substrate. Therefore, the CBD method causes larger thickness deviation of Sb_2S_3 layer and it makes difficult for the Sb_2S_3-SSCs to show reproducible device performance with narrow efficiency deviation. It is also considered that the formation of antimony oxides is indispensable when we deposit the Sb_2S_3 layer through aqueous phase chemical reaction.

On the other hand, the ALD process does not include any oxygen sources through entire chemical reactions and consequently it is expected that the formation of antimony oxides will be greatly suppressed. The thickness of Sb_2S_3 layer on bl-TiO_2/FTO substrate can be also precisely controlled as shown in Figure 1b because the formation of Sb_2S_3 is physically controlled by the repeated chemical reaction of the specific amount of precursors.

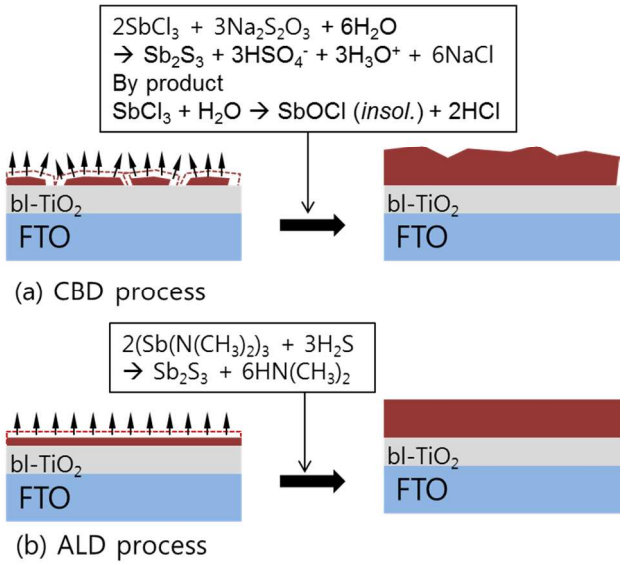

Fig. 1 Schematic illustration for the formation of Sb_2S_3 thin-layer on the bl-TiO_2/FTO substrate by CBD and ALD process.

Figure 2a and 2b show the typical cross-sectional TEM images of Sb_2S_3/bl-TiO_2/FTO substrate. Compared with the CBD-Sb_2S_3, the ALD-Sb_2S_3 thin layer with about 90 nm-thickness was more uniformly deposited along on the rough FTO/dense-TiO_2 surfaces. The magnified image of each inset shows that the ALD-Sb_2S_3 film is more densely formed than the CBD-Sb_2S_3 film because the later exhibited some pores within the film structure, which may formed by the thermal annealing process to convert its amorphous phase to crystalline one because the particle-like amorphous Sb_2S_3 are aggregated to form the film structure and they are converted into polycrystalline film through volume shrinkage by phase change. One of the merits of ALD process is the precise control of the thin film deposition by controlling ALD cycles. In order to investigate the

deposition rate of Sb_2S_3 thin films by ALD process, we measured the thickness of Sb_2S_3 thin films with the number of ALD cycles as shown in Figure 2c. From the thickness data quantified by spectroscopic ellipsometry, it was found that the thickness of Sb_2S_3 thin films linearly depends on the number of ALD cycles up to 4000 and the deposition rate of Sb_2S_3 was about 0.56 Å /cycle. As expected, this confirms that the ALD process can very reproducibly deposit the Sb_2S_3 thin films which will enable the Sb_2S_3-SSCs to have reproducible device efficiency. Meanwhile, the thickness of CBD-Sb_2S_3 films exhibited exponential increase with the deposition time and larger thickness-deviation than that of ALD-Sb_2S_3 which implies that the device will also have larger efficiency-deviation.

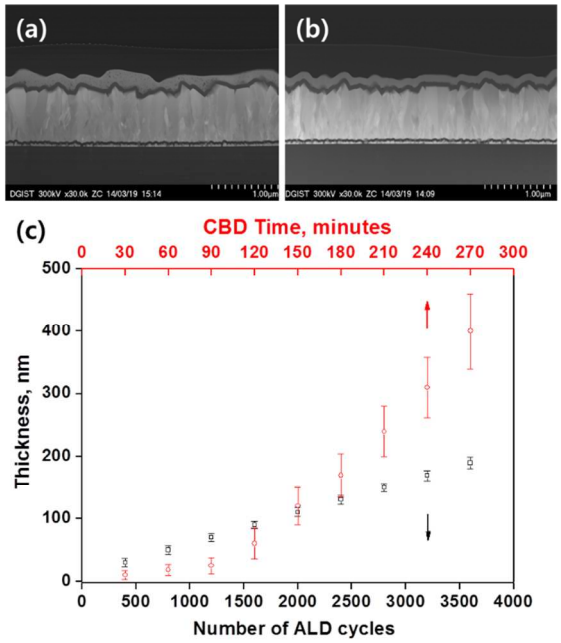

Fig. 2 A representative cross-sectional TEM image of (a) CBD-Sb_2S_3 (90nm ± 30nm) and (b) ALD-Sb_2S_3 (90nm ± 6nm) formed on bl-TiO_2 (~70nm)/FTO (450nm); and (c) the thickness of Sb_2S_3 layer deposited on a bare glass plate by ALD and CBD process.

The purity of Sb_2S_3 sensitizer is very important because the conventional CBD-Sb_2S_3 formed in aqueous phase synthesis yields the formation of antimony oxide and subsequently the deep traps below 1.03eV[19] from its conduction band energy are formed. The deep traps lead the injected electrons into TiO_2 electron conductor from Sb_2S_3 sensitizer to be transferred backward direction and cause the recombination of electrons and holes while deteriorating the open circuit voltage (V_{oc}). Therefore, we checked the purity of CBD-Sb_2S_3 and ALD-Sb_2S_3 by using X-ray photo electron spectroscopy (XPS) spectra as shown in Figure 3. Figure 3a shows that the deconvolution of the Sb 3d core level exhibits two chemical states of Sb_2S_3 (1 and 1′), Sb_2O_3 (2 and 2′) and an overlapping oxygen peak (3). These spectra clearly confirm that the Sb_2S_3 thin films deposited by conventional aqueous CBD process contains some amount of oxide. However, XPS spectra of Sb_2S_3 deposited by ALD process showed single peaks, which are single chemical state of Sb_2S_3 (1 and 1'), and there was no oxide and oxygen peak as shown in Figure 3b[22, 24]. From these XPS analysis, it was found that high quality Sb_2S_3 thin films without any oxide or oxygen impurities could be successfully deposited by ALD process, which might be advantageous for achieving high performance Sb_2S_3 solar cell.

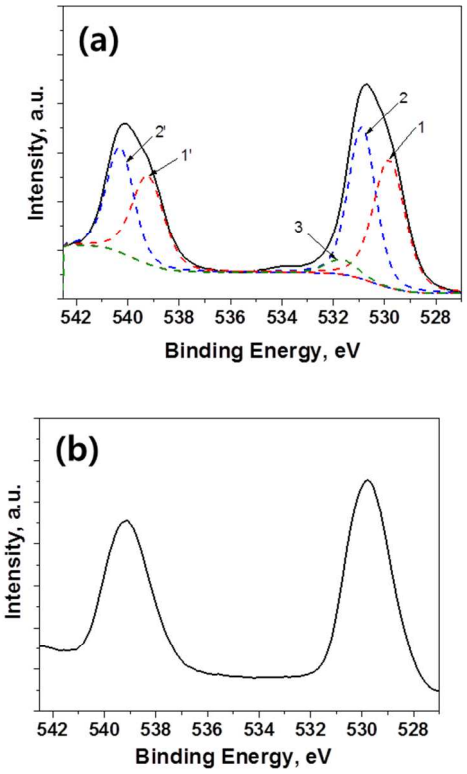

Fig. 3 XPS Sb 3d spectra of Sb_2S_3 obtained from the (a) conventional CBD process and (b) ALD process. The solid line is experimental data and dot line is fitted data. 1 (Sb_2S_3) = Sb 3d5/2, 1′(Sb_2S_3) = Sb 3d3/2, 2 (Sb_2O_3) = Sb 3d5/2, 2′ (Sb_2O_3) = Sb 3d3/2, 3 = O 1s.

Figure 4a shows the diffuse reflection spectra of ALD-Sb_2S_3 with the number of repeated ALD cycles where the thickness of ALD 400, 1000, 1600, and 2200 cycles correspond to 30nm ± 6nm, 60nm ± 7nm, 90nm ± 6nm , and 120nm ± 7nm. The absorption tail is gradually red-shifted with the thickness of ALD-Sb_2S_3 layer and almost is saturated over ALD 1600 cycles. Figure 4b and Table 1 show the current density-voltage (J-V) curves and the photovoltaic parameters (short circuit current density, open circuit voltage, fill factor, and power conversion efficiency: J_{sc}, V_{oc}, FF, and η) of CBD- and ALD-Sb_2S_3 devices. A conventional FTO/bl-TiO_2/CBD-Sb_2S_3/P3HT/Au device showed V_{oc} of 0.4886 V, J_{sc} of 9.63 mA/cm^2, FF of 46.13%, and η of 2.17 %, which are a similar result with previously reported planar Sb_2S_3-SSCs (V_{oc}=0.56V, J_{sc}=7.15mA/cm^2, FF=35%, η =1.43%)[25]. Here, it is noted that the CBD 120min sample exhibited the best device efficiency when we checked the efficiency of planar Sb_2S_3-SSCs with the CBD time (the thickness of CBD-Sb_2S_3 120min sample is shown in Figure 2a).

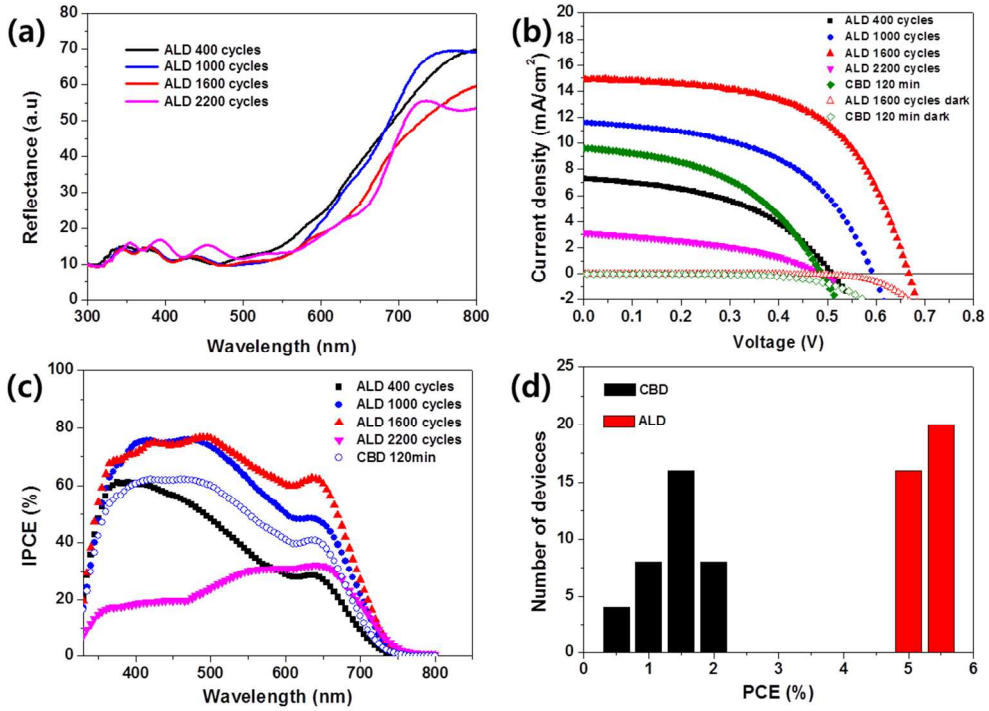

Fig. 4 (a) Diffuse reflection spectra of ALD-Sb_2S_3 deposited on a bl-TiO_2/FTO substrates for various ALD cycles, (b) current density-voltage (J-V) curves, and (c) IPCE spectra of planar FTO/bl-TiO_2/Sb_2S_3/P3HT/PEDOT:PSS/Au fabricated with different ALD cycles and by CBD 120min; and (d) PCE distribution of 36 planar Sb_2S_3-SSC samples fabricated by ALD 1600 cycles and CBD 120min.

Table 1. Summary of device performance for planar Sb_2S_3-SSCs. *Metal mask (0.096 cm^2) was attached to each cell before measurement under illumination (100 mW/cm^2).

Sb_2S_3 (cycles)	V_{oc} (V)	J_{sc} (mA/cm^2)	FF (%)	η (%)
ALD 400	0.5105	7.28	46.17	1.72
ALD 1000	0.5937	11.60	51.15	3.52
ALD 1600	0.6665	14.92	58.04	5.77
ALD 2200	0.4872	3.13	40.54	0.62
CBD 120min	0.4886	9.63	46.13	2.17

On the other hand, FTO/bl-TiO_2/ALD-Sb_2S_3/P3HT/Au devices exhibited dramatically enhanced photovoltaic performance, depending on the ALD cycles of Sb_2S_3; the J_{sc} enhanced with the increased ALD cycle of Sb_2S_3 up to 1600 cycles and then decreased with further increase in the ALD cycle. We also confirmed the enhancement of V_{oc} with an increase of the ALD cycle of Sb_2S_3 up to 1600 cycles and then a decrease of V_{oc} with the 2200 ALD cycle. All of ALD-Sb_2S_3 solar cells showed higher V_{oc} value compared with CBD-Sb_2S_3, which might be attributed to the formation of more pure Sb_2S_3 absorbers without impurities as confirmed by XPS analysis in Figure 3. The best device under air mass 1.5 global (AM 1.5G) full sunlight (100 mW/cm^2) exhibited J_{sc}, V_{oc}, and FF values of 14.92 mA/cm^2, 0.667 V, and 58.04 %, respectively, yielding η of 5.77%, which is three-fold higher than that of CBD Sb_2S_3 device.

In order to investigate the light response of Sb_2S_3 devices, we measured IPCE (Incident photon-to-current conversion efficiency) of CBD-Sb_2S_3 and ALD-Sb_2S_3 thin film solar cells (Figure 4c). Compared with CBD-Sb_2S_3, ALD-Sb_2S_3 solar cell with 1000 and 1600 ALD cycle showed higher IPCE, although the absorption spectra edge of CBD-Sb_2S_3 and ALD-Sb_2S_3 was same as near 750 nm-wavelength because the average thickness of Sb_2S_3 (CBD 120min and ALD 1000 cycles) was same to ~90 nm (see Figure 2a and 2b).

It should be noted that in spite of planar type solar cells, the planar ALD-Sb_2S_3-SSCs exhibited excellent photovoltaic performance compared with the planar CBD-Sb_2S_3 device and the mesoscopic CBD-Sb_2S_3-SSCs with P3HT hole conductor[26]. The improved performance of ALD-Sb_2S_3 solar cells might be attributed to the high purity Sb_2S_3 absorbers compared with conventional CBD-Sb_2S_3 absorbers because (1) the dark current leakage of ALD-Sb_2S_3 sample could be blocked even at higher bias voltage than the CBD-Sb_2S_3 sample as shown in Figure 4b and consequently enables the ALD-Sb_2S_3 to have higher V_{oc}[27]; and (2) the charge transfer and/or the charge collection efficiency of the ALD-Sb_2S_3 sample could be greatly improved than the CBD-Sb_2S_3 sample owing to the similar light harvesting efficiency by same thickness of Sb_2S_3 absorber where IPCE is product of light harvesting efficiency, charge transfer efficiency, and charge collection efficiency.

From thickness analysis of ALD-Sb_2S_3 thin films (Figure 2), it was found that the controllability and uniformity of ALD-Sb_2S_3 was much better than the conventional CBD-Sb_2S_3. This reproducible formation of Sb_2S_3 with small thickness-deviations by ALD process will guarantee the reproducible solar cell devices with small efficiency-deviations, which is a crucial factor for commercialization of solar cells. To confirm the reproducibility of solar cell devices, PCE (η) histogram of each individually fabricated solar cell devices

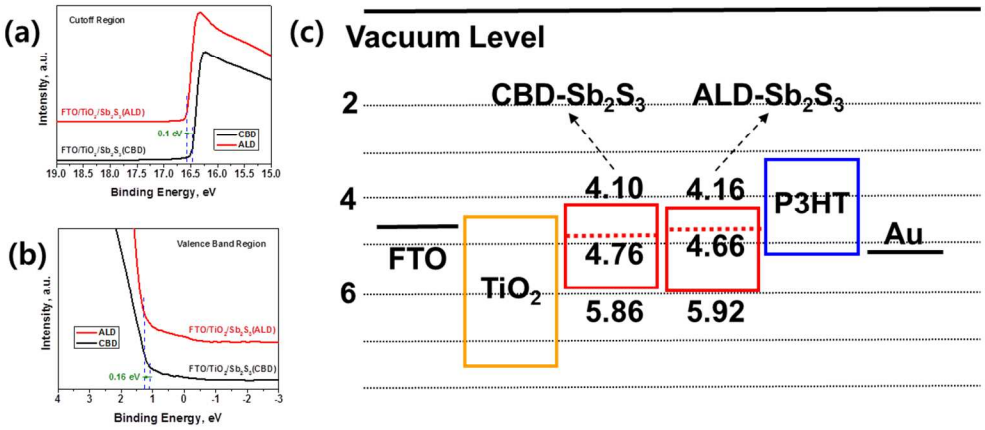

Fig. 5 UPS spectra at a) cutoff region, and (b) valance band region for FTO/bl-TiO_2/ALD-Sb_2S_3 and FTO/bl-TiO_2/CBD-Sb_2S_3 samples; and (c) corresponding energy band diagram of planar ALD-Sb_2S_3- and CBD-Sb_2S_3-SSC.

using CBD-Sb_2S_3 and ALD-Sb_2S_3 was exhibited in Figure 4d. The PCE histogram indicates that ALD-Sb_2S_3 solar cells show not only higher PCE but also narrow distribution of PCE compared with CBD-Sb_2S_3 solar cells. This result shows that the ALD process for the formation of Sb_2S_3 absorbers is a promising fabrication tool for the very reproducible solar cells.

Figure 5a and 5b show the UPS spectra of Sb_2S_3 films deposited on bl-TiO_2 by CBD and ALD process. The work function is determined from the photon energy and high binding energy cutoff of the UPS spectrum corrected for -5 V bias. The high binding energy cutoff is 16.56 and 16.46 V for ALD-Sb_2S_3 and CBD-Sb_2S_3, respectively (Figure 5a), and low binding energy onset of ALD-Sb_2S_3 and CBD-Sb_2S_3 is 1.26 and 1.10 V, respectively (Figure 5b). The work function was calculated by the equation, $\Phi = 21.22 -$ high binding energy cutoff, giving the position of Fermi level as 4.66 and 4.76 eV for ALD-Sb_2S_3 and CBD-Sb_2S_3, respectively. By adding the low binding energy onset in UPS spectrum, the valence band maximum with respect to the vacuum level can be calculated. The conduction band minimum is determined by adding optical band gap of Sb_2S_3, 1.76 eV, which is estimated from IPCE spectra (Figure 4c). From these results, it was possible to illustrate the energy band diagram of ALD-Sb_2S_3 and CBD-Sb_2S_3 devices (Figure 5c). The ALD-Sb_2S_3 showed 0.1 eV higher Fermi level compared with the CBD-Sb_2S_3, which might be attributed to the formation of pure Sb_2S_3 sensitizer by the ALD process because the oxide impurities make defect states in Sb_2S_3 absorbers and consequently the V_{oc} is deteriorated. Therefore, higher V_{oc} of ALD-Sb_2S_3–SSCs than CBD-Sb_2S_3-SSCs as shown in Figure 4 and Table 1 could be explained by the higher Fermi-level of ALD-Sb_2S_3 absorber.

Conclusions

We could fabricate reproducible planar Sb_2S_3-SSCs with 5.77% of power conversion efficiency with narrow efficiency-deviation by ALD technique whereas the planar Sb_2S_3-SSCs fabricated by conventional CBD method exhibited the poor power conversion efficiency with wide deviation. The high reproducibility of ALD-Sb_2S_3-SSCs was attributed to the conformal deposition of very uniform Sb_2S_3 thin-layer with narrow deviation on bl-TiO_2/FTO substrate meanwhile the CBD method yielded the formation of rough Sb_2S_3 thin-layer with wide deviation because the deposition rate of Sb_2S_3 thin-layer is nonlinear to reaction time and very sensitive to reaction temperature. The high device efficiency was attributed to the formation of pure Sb_2S_3 without oxide because oxygen source is not involved through entire ALD process while the aqueous phase based CBD inevitably forms antimony oxide. Therefore, the ALD-Sb_2S_3-SSCs exhibited high open circuit voltage, short circuit current density, and fill factor owing to the reduced backward recombination by greatly suppressed oxide defects within Sb_2S_3-sensitizer

Acknowledgements

This work was supported by DGIST R&D Program of the Ministry of Education, Science and Technology of Korea (14-EN-03).

Notes and references

[a] Energy Research Division, Daegu Gyeongbuk Institute of Science & Technology, 333, Techno jungang-daero, Hyeonpung-myeon, Dalseong-gun, Daegu 711-873, Republic of Korea

[b] Department of Chemical Engineeering, Kyung Hee University, 1732, Deogyeong-daero, Giheung-gu, Yongin-si, Gyeonggi-do 446-701, Republic of Korea

* E-mail: imromy@khu.ac.kr, sjsung@dgist.ac.kr

Tel.: (+82) 53-785-3700
Fax: (+82) 53-785-3739

[§] These two authors have equally contributed to this work.

Electronic Supplementary Information (ESI) available: [details of any supplementary information available should be included here]. See DOI: 10.1039/b000000x/

1 B. O'regan, M. Grfitzeli, *Nature*, 1991, **353**, 737.
2 S. Mathew, A. Yella, P. Gao, R. Humphry-Baker, B. F. Curchod, N. Ashari-Astani, I. Tavernelli, U. Rothlisberger, M. K. Nazeeruddin, M. Grätzel, *Nature Chem*., 2014, **6**, 242.
3 A. J. Nozik, *Chem. Phys. Lett*., 2008, **457**, 3.

4 R. Costi, A. E. Saunders, U. Banin, *Angew. Chem. Int. Ed*., 2010, **49**, 4878.
5 Y. L. Lee, Y. S. Lo, *Adv. Funct. Mater*., 2009, **19**, 604.
6 J. H. Bang, P. V. Kamat, *Adv. Funct. Mater*., 2010, **20**, 1970.
7 S. H. Im, Y. H. Lee, S. I. Seok, *Electrochim. Acta*, 2010, **55**, 5665.
8 S. H. Im, Y. H. Lee, S. I. Seok, S. W. Kim, S.-W. Kim, *Langmuir*, 2010, **26**, 18576.
9 S. H. Im, H.-j. Kim, S. W. Kim, S.-W. Kim, S. I. Seok, *Energy Environ. Sci.*, 2011, **4**, 4181.
10 J. Jean, S. Chang, P. R. Brown, J. J. Cheng, P. H. Rekemeyer, M. G. Bawendi, S. Gradečak, V. Bulović, *Adv. Mater*., 2013, **25**, 2790.
11 J. Y. Kim, O. Voznyy, D. Zhitomirsky, E. H. Sargent, *Adv. Mater*., 2013, **25**, 4986.
12 Y. Itzhaik, O. Niitsoo, M. Page, G. Hodes, *J. Phys. Chem. C*, 2009, **113**, 4254.
13 S.-J. Moon, Y. Itzhaik, J.-H. Yum, S. M. Zakeeruddin, G. Hodes, M. Grätzel*, J. Phys. Chem. Lett.*, 2010, **1**, 1524.
14 S. H. Im, H.-j. Kim, J. H. Rhee, C.-S. Lim, S. I. Seok, *Energy Environ. Sci.*, 2011, **4**, 2799.
15 S. H. Im, C.-S. Lim, J. A. Chang, Y. H. Lee, N. Maiti, H.-J. Kim, M. K. Nazeeruddin, M. Grätzel, S. I. Seok*, Nano Lett*., 2011, **11**, 4789.
16 Y. C. Choi, Y. H. Lee, S. H. Im, J. H. Noh, T. N. Mandal, W. S. Yang, S. I. Seok, *Adv. Energy Mater.*, 2014, **4**, 1301680.
17 K. Tsujimoto, D.-C. Nguyen, S. Ito, H. Nishino, H. Matsuyoshi, A. Konno, G. R. A. Kumara, K. Tennakone, *J. Phys. Chem. C*, 2012, **116 (25)**, 13465.
18 S. Ito, K. Tsujimoto, D.-C. Nguyen, K. Manabe, H. Nishino, *International Journal of Hydrogen Energy*, 2013, **38**, 16749.
19 Y. C. Choi, D. U. Lee, J. H. Noh, E. K. Kim, S. I. Seok, *Adv. Funct. Mater.*, 2014, **24**, 3587.
20 S. Messina, M. Nair, P. Nair, *Thin Solid Films*, 2007, **515**, 5777.
21 D. U. Lee, S. W. Pak, S. G. Cho, E. K. Kim, S. I. Seok*, Appl. Phys. Lett*., 2013, **103**, 023901.
22 N. Maiti, S. H. Im, C.-S. Lim, S. I. Seok, *Dalton Trans*., 2012, **41**, 11569.
23 H. Wedemeyer, J. Michels, R. Chmielowski, S. Bourdais, T. Muto, M. Sugiura, G. Dennler, J. Bachmann, Energy Environ. Sci., 2013, 6, 67.
24 C. P. Liu, H. E. Wang, T. W. Ng, Z. H. Chen, W. F. Zhang, C. Yan, Y. B. Tang, I. Bello, L. Martinu, W. J. Zhang, S. K. Jha, *Phys. Status Solidi B*, 2011, **249**, 627.
25 P. P. Boix, Y. H. Lee, F. Fabregat-Santiago, S. H. Im, I. Mora-Sero, J. Bisquert, S. I. Seok, *ACS Nano*, 2011, **6**, 873.
26 J. A. Chang, S. H. Im, Y. H. Lee, H.-j. Kim, C.-S. Lim, J. H. Heo, S. I. Seok, *Nano Lett*., 2012, **12**, 1863.
27 J. Y. Hwang, S. A. Lee, Y. H. Lee, S. I. Seok, *ACS Appl. Mater. Interfaces*, 2010, **2**, 1343.

